Article:
Escudero-Castejón, L, Taylor, J, Sánchez-Segado, S et al. (1 more author) (2021) A novel reductive alkali roasting of chromite ores for Carcinogen-free Cr6+-ion Extraction of chromium oxide (Cr2O3) – a clean route to chromium product manufacturing! Journal of Hazardous Materials, 403. 123589. ISSN 0304-3894

https://doi.org/10.1016/j.jhazmat.2020.123589

A novel reductive alkali roasting of chromite ores for Carcinogen-free Cr^{6+}-ion Extraction of chromium oxide (Cr_2O_3) – *a clean route to chromium product manufacturing!*

Lidia Escudero-Castejón, James Taylor, Sergio Sánchez-Segado, Animesh Jha*

School of Chemical and Process Engineering
Faculty of Engineering, University of Leeds, Woodhouse Lane, Leeds LS2 9JT
*: corresponding author a.jha@leeds.ac.uk

Abstract

A novel reduction reaction for extracting Cr_2O_3 from chromite ores is demonstrated by excluding the formation of carcinogenic chromate (Cr^{6+}) intermediates. We have investigated in detail the underpinning high-temperature reduction reaction: $FeCr_2O_4+Na_2CO_3+2[C]=[Fe]+Na_2Cr_2O_4+3CO_{(g)}$, which defines the process chemistry for the formation of sodium chromite (Na_2CrO_2) as an intermediate product for Cr_2O_3 extraction. After high-temperature reduction, the magnetic separation, aqueous and acid leaching of reaction products yielded 81 wt% and 70 wt% pure Cr_2O_3 from low (~4 wt%) and high (>8 wt%) silica-containing chromite ores, respectively. The process diagram explains the extraction of Cr_2O_3, Fe-Cr alloy, Al_2O_3, and MgO-Al_2O_3-silicate, reuse of CO_2 for Na_2CO_3 recovery, and energy generation from CO combustion for demonstrating Cr^{6+}-free extraction of metallic and mineral values from chromite ores.

The process chemistry demonstrates the extraction of 75-80% pure Cr_2O_3 from $NaCrO_2$ by leaching with 0.05-0.5M dilute H_2SO_4 in controlled pH conditions. The detailed chemical analysis of leachates after Cr_2O_3 extraction shows that the acid leachates with residual concentrations of ~150 ppm Cr^{3+}-ions can be recycled in situ for reusing water, for eliminating the risk of Cr^{6+}-ion formation from atmospheric oxidation. The novel extraction route may be able to displace the current oxidative process for chromite ore processing by retrofitting.

Keywords: chromium, chromite ore, reductive roasting, chromite reduction, iron-chromium alloy, chromium oxide chemicals, Cr^{6+}-ion analysis, Cr^{6+}-ion carcinogen, process design.

1). Introduction

1.1 Oxidative process chemistry of chromite roasting in the presence of alkali

Chromium is an important metallic element, known for high and low temperature corrosion and oxidation-resistance properties, which the element imparts to the stainless steel and superalloys [1]. Other usages of chromium are in the production of chemicals [2, 3] for manufacturing dyes and pigments, tanning of leather, chrome plating and catalysts [4].

The traditional route for manufacturing chromium products is based on the extraction of chromium oxide as sodium chromate via the oxidative alkali roasting of chromite ores, in air or oxygen. The generic chemical reaction for chromite to sodium chromate may be explained by considering the oxidation of iron chromite ($FeCr_2O_4$), as shown below in reactions (1). In this reaction, the iron chromite ($FeCr_2O_4$) is the main Cr^{3+}-ion bearing spinel in a quaternary solid-solution of three other spinels in natural chromite [5, 6]. Besides $FeCr_2O_4$, the other commonly present spinels are: $MgO.Al_2O_3$, $MgO.Cr_2O_3$ and $MgO.Fe_2O_3$. Refractory oxides (CaO, MgO, Al_2O_3, SiO_2) form gangue minerals in natural chromite ores.

$$2FeCr_2O_4 + 4Na_2CO_3 + 3.5O_2(g) = 4Na_2CrO_4 + 4CO_2(g) + Fe_2O_3 \qquad (1)$$

Since the discovery of the process in 1885 by Le Chatelier, the presence of oxygen and alkali is necessary for the oxidative decomposition of chromite at high temperatures (900-1150ºC) [5-8]. The process chemistry of sodium chromate manufacturing has remained mostly unchanged since 1885, except the hazardous and carcinogenic nature of Cr^{6+}-ions became apparent in the 20th century, with the increasing use of chemicals for oxidation-resistant coatings. As explained above, the chromite ores invariably have silica (1-10wt%) and lime. These two oxides are considered critical in the feedstock analysis for chromium chemicals extraction [6-8]. Silica forms viscous eutectic liquid above 900ºC, which impedes oxygen mass transport [5,8]. Consequently, the reaction (1) suffers from oxygen starvation, and stop before completion, which leaves the unreacted chromite ore process residue (COPR) as a waste [9-12]. In chromite ores with less than 3 wt% silica, the proportion of COPR is much reduced than that in high silica (>5 wt%) ores. Waste handling, management, and monitoring costs of COPR [9,11,12] is invariably high, as it may contain more than 2 wt% of hazardous and carcinogenic sodium chromate [9-12], which is highly soluble in water.

1.2) Legacy of Environmental Issues and Management

In today's world, the legacy of processing low and high-silica chromite continues to be environmentally challenging, due to the reliance on landfilling and sealing of COPR in

many parts of the world. Before 1970, the processing of high-silica chromite ores required the use of dolomite or lime for complexing with silicates at high temperatures. However, lime also formed volatile and readily water-soluble Cr^{6+}-ion containing calcium chromate ($CaCrO_4$). Both Na_2CrO_4 and $CaCrO_4$ were found present in lime-rich COPR [9] at nearby landfill sites where the chromate chemicals were processed. An example in **Figure 1** illustrates the microporous structures of unreacted and leached sodium chromate COPR, from which the hazardous Cr^{6+}-ions are slowly released into the surrounding environment, posing a significant threat to living species from exposure. It is this risk of COPR defines the "*unmet challenge for sustainable and responsible manufacturing of chemicals*" [10-12]. For most of the chromite ores, the extraction efficiency for chromite to Na_2CrO_4 by oxidative roasting with Na_2CO_3 remains below 90%, as summarised in Table 1. However, amongst the chromite ores, the S African ores yield nearly 90% of sodium chromate, which is the highest value of extraction efficiency known in the literature [5,7-11], as it contains low SiO_2 (0.98 wt.% SiO_2 from the Bushveld deposits) [10].

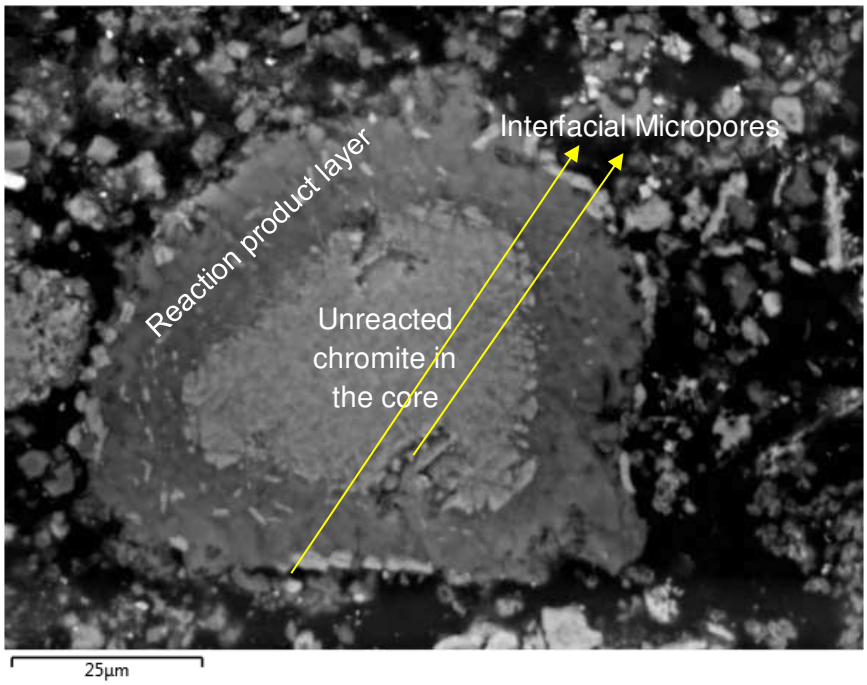

Figure 1: A backscattered SEM micrograph of a partially-reacted particulate of South African chromite ore, roasted with the stoichiometric amount of NaOH for 2 hours at 1000°C in air atmosphere and subsequent leaching with water at 50°C. The SEM cross-section shows the unreacted chromite core surrounded by the reaction product. The micropores (see arrows) present in the cross-section form because of the molar volume change during the chemical reaction.

Table 1 presents and compares a summary of the percentage yield of Na_2CrO_4 from different types of chromites after high-temperature oxidative roasting, followed by water leaching and residue washing. In industry, the extraction efficiency of water-soluble chromate from COPR is quantified for determining the risk of Cr6+-ion released into the environment [11, 12]. The tonnage COPR data in Table 1 emphasizes the need for

reducing future dependency on landfilling for protecting land (L), air (A) from dust, water (W) from seepage. Consequently, the lime-based oxidative process was abandoned globally by the industry. Instead, the increased alkali process by using either Na_2CO_3 or NaOH was implemented [2,9]. In the proposed article, we explain a hexavalent chromium hazard-free methodology for the extraction of chromium chemicals, which also protect the land, air, and water (LAW) by eliminating the risk of exposure of Cr^{6+}-ions to living species.

Table 1. Experimentally reported yield of Na_2CrO_4 from chromite ores of different mineralogical origins, extracted using alkali roasting with Na_2CO_3 in air and leaching with water [10].

Chromite ore origin	**South Africa**	**India**	**Philippines**	**Indonesian**	**Chinese**
% yield of Na_2CrO_4	90	63	75	58	42
kg of COPR per tonne of chromite	469.5	620.1	538.2	639.3	753.4

Several authors have investigated the catalytic oxidative roasting and leaching using potassium hydroxide (KOH) in autoclaves [13, 14] in the temperature range of 30-200^oC for selectively separating water-soluble potassium chromate. Note that, based on the oxidative reaction 1 and irrespective of any extraction methodology adopted for the extraction of alkali chromate (e.g. Na_2CrO_4), the chromate reaction (1) never yields COPR which is safe for disposal. This is because of the high concentrations of residual Cr^{6+}-ions in COPR, which is not able to meet the regulatory requirement for environment safety, waste management and monitoring of hazardous Cr^{6+}-ions. For preventing the risk of leakage and seepage, the capping of landfills and continued monitoring is the only expensive alternative. The US Environmental Protection Agency and World Health Organisation require monitoring compliance in the 10 and 50 parts per billion (ppb), respectively [15] [16]. Even at such low ppb concentrations, the long-term genetic and cellular damage to plants and animals and environmental risks are still unknown [17].

In this article, we demonstrate a novel reductive route for chromium oxide (Cr_2O_3), iron-chromium alloy and alumina extraction from chromite. The novel route for chromium product extraction and further purification offers an alternative solution for the ongoing and unmet challenge of landfilling and monitoring COPR. We also demonstrate that the spent leachate is a dilute sulphuric acid with 0.05M-0.5M strength at the end of the process, which contains little or no Cr^{6+}-ions immediately after processing. By leaving the acid leachate in air for several weeks, the residual Cr^{3+}-ions oxidize and yield Cr^{6+}-ions up to 140 ppm. In this investigation, we demonstrate a close loop process for the reuse of spent leachate for water recycling into the leaching part of the overall process for demonstrating a “hazard-free chemistry” approach. The article also explains the energy and environmental benefits of reductive roasting of chromite, which has potential for displacing the traditional oxidative process by introducing minimal disruption to the

process infrastructure. Since the overall manufacturing setup is likely to remain unchanged, by switching to reduction route with retrofitting will remove the need for dependency on landfill dependency for COPR handling and management.

1.3) Novel Reduction Chemistry of Alkali Reaction with Chromite Ores

For reductive roasting of chromite ores with alkali, the presence of a reducing agent, e.g. carbon is necessary, which is in contrast with the oxidation process, shown in reaction 1. Under the reducing condition, the alkali complexes with chromium oxide in 3+-state and forms water-insoluble sodium chromite ($Na_2O{\cdot}Cr_2O_3$). Iron oxide present in the chromite spinel is reduced to a metallic state by forming Fe-Cr alloy, whereas the alumina forms water-soluble $NaAlO_2$. The water-insoluble sodium chromite may be separated during leaching from the soluble $NaAlO_2$. The residual oxides, MgO, Al_2O_3 and silica form complex silicates during leaching. For comparing the stable phases formed during reduction reaction with that in the oxidative reaction (1), we have considered the $FeCr_2O_4$ in the complex spinel as the dominant source of Cr^{3+}-ions for the formation of $NaCrO_2$ extraction $(Mg,Fe^{2+})[Al,Cr,Fe^{3+}]_2O_4$. The Gibbs Energy ($\Delta G^o$, $J.mol^{-1}$) change for competing chemical reduction reactions with alkali and the equilibrium temperatures (T_{eq}, K) are shown in Table 2.

Table 2: The temperature-dependent equations for the Gibbs Energy **(ΔG^o, J mol^{-1})** change for competing reduction reactions during the alkali-assisted decomposition of iron chromite spinel ($FeCr_2O_4$) and complexation of gangue minerals (Al_2O_3, SiO_2, and MgO).

Equation number for Chemical reactions	(ΔG^o, J mol^{-1})	T_{eq},K
2). $FeCr_2O_4+Na_2CO_3+2C=Fe+ Na_2Cr_2O_4 + 3CO(g)$	466,491-44.3T	1048
3). $Al_2O_3 + Na_2CO_3 + C = 2NaAlO_2 + 2CO$ (g)	337267-287.2T	1174
4). $Na_2CO_3 + SiO_2 + C = Na_2SiO_3 + 2CO$ (g)	284162-299.0T	950
5). $MgCr_2O_4+Na_2CO_3+C = MgO+ Na_2Cr_2O_4+2CO(g)$	321105-289.2T	1110
6). $FeAl_2O_4+Na_2CO_3+2C = Fe+2NaAlO_2+3CO(g)$	313087-286.4T	1093
7). $MgAl_2O_4 + Na_2CO_3 + C = MgO + 2 NaAlO_2 + 2CO(g)$	315522-285.2T	1106
8). $MgSiO_3+Na_2CO_3+C=MgO+Na_2SiO_3+2CO(g)$	268000-287.4T	932
9). $CaO.Al_2O_3.2SiO_2+3Na_2CO_3+3C=2Na_2SiO_3+2NaAlO_2+CaO+6CO(g)$	207880-205.5T	1011

In Table 2, for each reaction, the value of equilibrium temperature, T_{eq} (K) was derived by equating the temperature-dependent ΔG^o equation to zero. From this table, it is evident that above 1174K the equilibrium shifts in the forward direction. In natural chromites, the $FeCr_2O_4$ and $MgCr_2O_4$ spinels bear the highest molar concentration of Cr_2O_3. During reduction, it is from these two spinels the $NaCrO_2$ and Fe-Cr alloy form above 900C. Also, the values of ΔG^o for the decomposition of $MgAl_2O_4$ and $FeAl_2O_4$ are much smaller than that for the formation of $NaCrO_2$, $NaAlO_2$ and Na_2SiO_3, which imply that the alkali complexes are more stable than the spinels [18-20]. The subsequent

separation of reaction products is based on the pH-dependent water solubility of $NaAlO_2$, Na_2SiO_3, and $NaCrO_2$.

By comparing the equilibrium for oxidative roasting in equation 1 with the reduction reactions in Table 2, the main process characteristics of the alkali roasting of chromite spine are discussed below:

i. The iron oxides present in chromite reduce to metal and form Fe-Cr alloy above 1173K (900^{o}C), which may be separated magnetically from the non-magnetic phases.

ii. Since $NaAlO_2$ and Na_2SiO_3 are soluble in water, the insoluble $NaCrO_2$ present in the non-magnetic fraction may be separated during leaching.

iii. As discussed below, the separation of aluminium hydroxide from water-soluble $NaAlO_2$ is known to occur in the presence of CO_2 gas [7]. The reduction reactions, discussed in Table 2, generate CO gas which **may** be used for combustion for energy generation. The CO_2 generated from CO gas combustion will be used for **the** recovery of Na_2CO_3 for reuse in the process. Since, most of the alumina and silica are left in COPR [8-12], the reclamation of these two oxides provides a step towards coproduct manufacturing, which then reduces the burden of waste disposal.

iv. The combustion of CO gas with oxygen generates a significant amount of energy for meeting the overall energy cost.

v. Since the separated $NaCrO_2$ remains free from Cr^{6+}-ions, it can be directly used for designing a manufacturing process for chromate and Cr_2O_3 chemicals, which will remove the need for the disposal of COPR and washed leachates.

In this article, we have investigated the kinetics of high-temperature reduction reactions (2) with alkali using the thermogravimetric analysis (TGA) [12], and the subsequent methods for purifying reaction products via leaching. Such analytical approaches will demonstrate and ensure that neither any solid nor any liquid waste has traceable quantities of hazardous Cr^{6+}-ions, which must be disposed safely. As explained in section 1.2 that the yield of chromium chemicals is dependent on the silica content of the chromite feedstock [5], however, in this investigation the low- and high-silica chromite ores from S Africa, and Brazil and Indonesia, respectively, have been specially chosen for characterizing the reductive alkali roasting reaction for the formation and separation of sodium chromite, alloy formation and alumina extraction reactions and products. The phase and chemical analyses of selected ores are shown in Table 3.

For overall analysis of the Cr^{6+}-bearing waste minimization, the regeneration of Na_2CO_3 during aluminium hydroxide regeneration by reusing CO_2 from the combustive oxidation of CO gas is also explained. The purity of reaction products was analysed using the X-ray powder diffraction (XRPD), scanning electron microscopy (SEM), energy-dispersive X-ray (EDX) and X-ray fluorescence (XRF). For trace concentration analysis of Cr^{3+} and Cr^{6+} ions in leachates, the atomic absorption (AA) and UV-visible (UV-vis) spectroscopic

techniques were used. A schematic of the process flow diagram showing the extraction routes for chromium ($NaCrO_2$, Fe-Cr alloy) and coproducts (e.g. alumina) is presented in the supplementary information (SI) **Figure S1**.

2) Computational and Experimental Methodologies

As discussed above in the context oxidative roasting that the overall concentrations of silica in chromite determines the grade and suitability of ore for the manufacturing of chromate chemicals. The proportion of alkali required to form alkali chromite in the reductive roasting reaction will depend on the silica content of chromite. For this reason, the detailed mineralogical characterization of chromite ores studied herein is important.

2.1) Materials characterization for chemical reaction

Since the most of Cr_2O_3 and iron oxides are present in the $FeCr_2O_4$ and $MgCr_2O_4$ fractions of natural chromite (see below Table 3), the reduction reactions (2)-(5) in Table 2 were considered for detailed phase analysis using the thermodynamic software packages Fact Sage and HSC [21, 22]. The reactions (6)-(9) in Table 2 are less significant for process analysis. In Table 3, the compositions, phases present, particle size range, density ($g.cm^{-3}$) and lattice dimensions (nm) of S. Africa, Brazilian, and Indonesian ores are compared.

2.2) Materials and Methods

Ore Mineralogy: The mineralogical phase analysis of chromite ores was carried out using XRPD, XRF, AA and electron probe micro-analysis (EPMA) techniques, and the average values of the analysed compositions are reported in Table 3. In this table, the composition range for each ore is shown by comparing the weight percent of Cr_2O_3 and SiO_2 present in the ore body. The mineralogical analysis of each ore shows three main constituents: **a**) quaternary spinel $(Fe_{0.52},Mg_{0.48})(Cr_{.76},Al_{0.24})_2O_4$, **b**) calcium- or magnesium-based gangue silicate minerals e.g. $Ca_{11.5}Al_{23}Si_{25}O_{96}$ in S African, hydrated silicates in Brazilian and $MgSiO_3$ in Indonesian, and **c**) liberated quartz (SiO_2). The silicate and quartz are undesirable for alloy and chemicals products. Some quaternary spinels also have trace quantities of TiO_2, V_2O_5 at the octahedral and MnO and CaO at the tetrahedral sites, respectively.

Reactants: Each ore was batched into 100g weight and mixed with the analytical grades (99.9% pure) of Na_2CO_3 and active charcoal in the weight ratio of chromite:Na_2CO_3: charcoal equal to 1:1:0.2. The reactants were mixed by grinding using a mortar and pestle for 10 minutes. The ground mixture of reactants was then pressed into 2g of pellet using a steel die. After pressing the pellet was placed inside an alumina crucible. Before starting the isothermal reduction experiment at a predetermined isothermal temperature for fixed time, e.g. 1050^oC for 2.5 hours, a vertical furnace with thermogravimetric balance (see **Figure S2**), was purged with argon gas, maintained at flow rate of 2 litres per minute for 15 minutes.

At the end of the TGA experiment, the reduced mixture was cooled down to room temperature. The phase analysis of reaction product was carried out using XRPD, XRF and SEM techniques. For magnetic separation, approximately 100g of reactant mixture was heat treated at 1050^{o}C for 2.5 hours in a muffle furnace purged with argon gas. For maximizing the separation of non-magnetic fraction from the magnetic Fe-Cr alloy, the reactant was washed down with water at 50^{o}C several times on a lab-scale magnetic separator (Wet Test Chute from Master Magnets Ltd). After magnetic separation, the dried reaction product was analysed using XRF, XRPD and SEM techniques for phase characterization. The non-magnetic fraction was acid leached at 50^{o}C for 1.5 hours, using 0.05-0.5M strength diluted sulphuric acid with a solid-to-liquid ratio of 1g:70mL. The residue after acid leaching of the non-magnetic fraction was analysed for residual Cr_2O_3 content.

The alkaline leachate from washing during magnetic separation was collected in a 1 litre vessel. The leachate was bubbled with the CO_2 gas maintained at a rate of 1 litre/minute flow rate, which initiated the precipitation of $Al(OH)_3$. The hydroxide was filtered out and the remaining solution was evaporated for crystallizing Na_2CO_3 for reuse in the process [23, 24]. The solid residue left after CO_2 sparging of $NaAlO_2$-bearing leachate was analysed for the presence of residual metallic constituents.

2.3) Isothermal Thermogravimetric analysis (TGA)

For mass balance and reduction reaction rate analysis of chromite, the TGA was carried out using a thermal balance (see Supplementary Information Fig.S2) [5], which had a sensitivity range in sub 100mg range. In each TGA analysis, 2g of pressed pellets with a stoichiometric mixture of chromite, Na_2CO_3 and activated charcoal (C) in a ratio of 1:1:0.2 was used for reaction rate analysis by characterizing the weight change (Δw,g) against time (t) at a chosen isotherm. The Δw against t plots are shown below. Besides isothermal TGA, non-isothermal experiments were also carried out for detailed mass balance analysis using 100g batch (See SI).

2.4) Chemical analysis of solid samples by XRF, XRD and SEM Analysis Techniques

For detailed chemical analysis of solid reactants and products, the XRF technique was adopted (see SI). The phase analysis of reacted and unreacted powder mixtures was carried out using XRD with Cu-K_α radiation (λ=0.15417nm). Each powder sample was scanned with a step size of 2θ=0.0334^{o} s^{-1} from 2θ=5^{o}-85^{o}. An example of the XRPD data with Rietveld refinement [25] for phase identification for the S African and Indonesian ore is presented in Figure S2 in SI. The SEM analysis was carried out using the Zeiss e-SEM, equipped with an X-ray detector for the elemental characterization of phases present.

2.5) UV-visible spectroscopic analysis of leachate solutions

For quantifying the residual concentrations of Cr^{3+} and Cr^{6+}-ions in the acid-leached media, discussed above, the UV-visible-NIR absorption spectroscopy was adopted using the Perkin-Elmer Lamda-950 model for concentration calibration and accurate quantification of oxidation states.

Table 3: Chemical analysis, phase constitution, particle size distribution (μm) and crystal structure of natural chromite spinel minerals

Properties of Naturally Occurring Chromite Spinel Ores	
Weight per cent (wt%)	S African Ore: Cr_2O_3- 44.8, Fe_2O_3-24.6, MgO-10.9, Al_2O_3-14.4, SiO_2-3.8, TiO_2-0.5, V_2O_5-0.3, MnO-0.3, CaO-0.4.
	Brazilian Ore: Cr_2O_3- 44.3, Fe_2O_3-14.4, MgO-15.1, Al_2O_3-16.1, SiO_2-8.5, TiO_2-0.25, CaO-1.34.
	Indonesian Ore: Cr_2O_3-43.4, Fe_2O_3-24.9, Al_2O_3-18.8, MgO-10.5, SiO_2-1.5, Mn_3O_4-0.3, TiO_2-0.5, CaO-0.1
Particle size range	90-110μm (S African); 90-120μm (Brazilian); 90-150μm (Indonesia)
Phase compositions	S African: $(Fe_{0.52},Mg_{0.48})(Cr._{76},Al_{0.24})_2O_4$, $Ca_{11.5}Al_{23}Si_{25}O_{96}$ and SiO_2.
	Brazilian: $Fe_{0.62}Mg_{0.38}Cr_{1.63}Al_{0.37}O_4$ (average from XRF & EPMA), $(Mg,Fe,Al)_6(Si,Al)_4O_{10}(OH)_8$, SiO_2, $NaCa_2Mg_5AlSi_7O_{22}(OH)_2$, $K_{0.7}Na_{0.4}Ca_{1.1}Al_{3.3}Si_{8.7}O_{24}(H_2O)_3$.
	Indonesian: Spinel phase composition range: Fe^{2+}: 0.35-0.76, Mg^{2+}: 0.23-0.64, Al^{3+}: 0.14-1.23, Cr^{3+}: 0.71-1.76, Fe^{3+}: 0.048-0.656, Ti^{4+}: 0.001-0.011; Silicates: $MgSiO_3$, SiO_2
Density (g cm^{-3})	3.728 (SA); 3.713-3.898 (Brazil); 4.201 (Indonesia)
Lattice parameter	Face-centred cubic/Fd-3m a=0.8306 nm (S Africa); a=0.8287 nm (Brazil); a=0.8211-0.8338 nm (Indonesia).

3) Results and discussion

3.1) Comparison of rates of reduction reaction for chromite ores

For comparing the rates of chromite reduction in the presence of alkali, the extent of reduction reaction (X) was calculated from the isothermal TGA data, which were collected in the range of 800°C-1050°C. The observed weight change (Δw,g) was recorded with time and compared with the stoichiometric weight loss (W_o,g). From the measured Δw at any instant of time t (in hours) and W_o, the value of fractional percentage (X,%) of the overall reaction was calculated using equation (eq.1), and the plotted against t in hours.

$$X = \frac{\Delta w}{w} x100 \qquad \text{eq. (1)}$$

The rates of reaction curves in Figures 2a and 2b are for the S African and Brazilian chromites, respectively. The plotted *X%* vs t data have a strong dependence on the reduction temperature. Above 950°C, the overall reaction reaches near completion in 2

hours, beyond which only a small change in weight was observed. On the other hand, at 950°C isotherm, a fractional gain in weight after 1.5 hours was observed, which was less evident at 1000°C after 3 hours. The weight gain in chromite reduction may be attributed to the carbon deposition via the Boudouard reaction: $2CO=CO_2+C$. Both the iron and iron-chromium alloys are known to form carbides in the 850°-1000°C range. Under saturation condition, the carbon deposits, and dissolves into the newly formed Fe-Cr alloy at and above 850°C, and helps in forming thermodynamically stable carbide (Fe_3C, Cr_xC_y) precipitates in the alloy matrix [27].

By comparing the reducibility of S African ore with the Brazilian ore, the overall weight gain due to the carbon deposition $2CO=CO_2+C$ reaction is less apparent between 900°C and 1000°C in **Figure 2b**. From the analysis of the overall rate of completion of reaction at different temperatures, it is apparent that the reduction reaction reaches up to X=95% for the S. African chromite at 1050°C. Whereas in the case of the Brazilian ore, the maximum extent of reducibility (X%) was found to be less than 75% at 1050°C. The initial rates of reaction for these two ores were also analysed by comparing the extent of reaction achieved in the first 60 minutes. From the comparison of X% data for the S African and Brazilian ores in Figures 2a and 2b, respectively, it is evident that more than 75% and 60% of the overall reaction completed in 1 hour at 950°C. From **Figures 2a and 2b**, the overall reduction reaction is divided into three regimes: a) *initial fast step*, b) *slower intermediate stage* and c) *a long tail of reaction termination*.

The analysis of reduction reaction for the Indonesian chromite ore in the presence of alkali was also investigated using the isothermal TGA with 2 grams of test samples. Besides the TGA analysis, 100g of reactant was taken for non-isothermal heating experiment in argon atmosphere in a muffle furnace. It was found that the value of fractional reduction (X%) was higher than 75% in less than 2.5 hrs at 1050°C. Once the detailed reaction kinetics data were selected chromite ores were also reduced in 1kg/hour kiln at 1050°C. The phase analysis results for the Indonesian ores were found to be consistent with the isothermal and non-isothermal data for the S African and Brazilian ores, as compared below.

3.2) Comparative Phase Analysis after High-temperature Reduction of Chromite Ores using X-Ray Powder Diffraction

The detailed phase analysis of reaction products was carried out using XRPD, SEM with EDX and further supplemented with XRF and EPMA techniques. **Figures 3a and 3b** are the XRPD data for the reduced S African and Brazilian ores, respectively. For Indonesian chromite, the XRPD of the reaction product was also compared with the unreacted ore (see Figures S3).

3.3) Computed equilibrium analysis of reduced chromite ores with alkali:

The phase analysis data in **Figures 3a and 3b** were also compared with the predicted phases in the predominance area diagram for in the Fe-Cr-Na-C-O, Mg-Cr-Na-C-O and Fe-Al-Na-C-O systems in **Figures 4**, Figures S4a and S4b, respectively. The predicted

equilibrium phase assemblages $Fe+NaCrO_2+Na_2CO_3$, $MgO+NaCrO_2+Na_2CO_3$, $Fe+NaAlO_2+Na_2CO_3$ are the most relevant which agree well with XRPD analysis. The XRPD and computed phase equilibria confirm that the reduction reaction does not alter the valence state of Cr^{3+}-ions which after reaction is present as $NaCrO_2$. The remaining chromium reduces to metal by forming the Fe-Cr alloy. The decomposition of spinel in the presence of alkali converts Al_2O_3 into a water-soluble compound, called the sodium aluminate ($NaAlO_2$). The XRPD in **Figure 3** (phases 6,7 and 8) shows the presence of a complex magnesium-aluminium-calcium-silicate, formed as a result of the thermal decomposition of spinel and complexation with alkali.

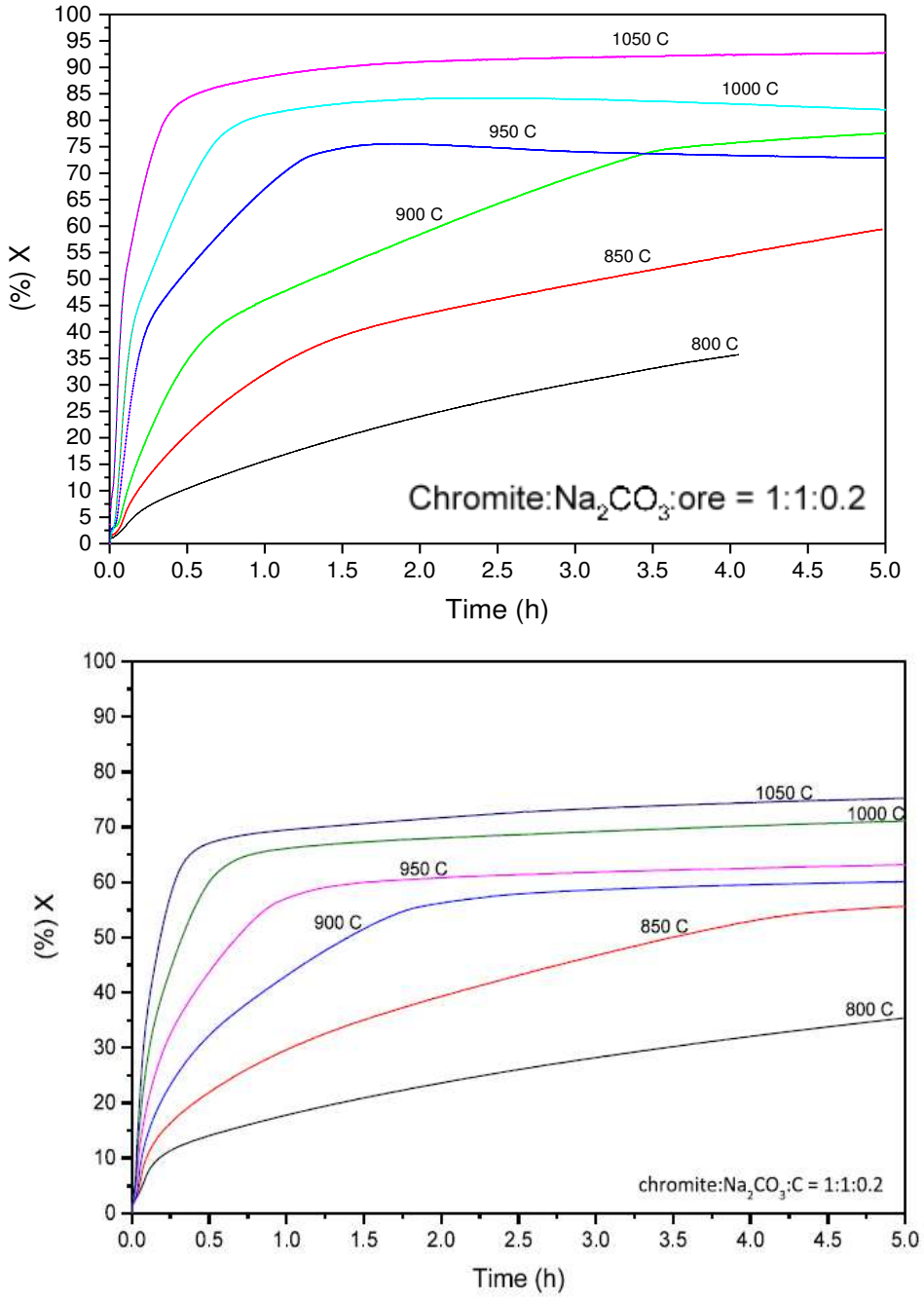

Figure 2: Percentage reduction (X,%) vs time (t, hour) curves for isothermal carbothermic reduction at constant temperatures (800°C, 850°C, 900°C, 950°C, 1000°C and 1050°C) with a chromite:Na_2CO_3:charcoal weight ratio of 1:1:0.2. (**a**) S. African chromite ore and **(b)** Brazilian chromite and (see Table 2) in the presence of Na_2CO_3.

Examples of the predominance area diagram are shown in **Figure 4** (also in Figures S4a-S4b). The apparent weight gain in **Figure 2a**, XRPD data in **Figure 3a** and the predominance diagram in **Figure 4** support the evidence for the formation of the complex carbides of Fe_3C and Cr_2C_3 via carbon deposition during the reduction reaction at 950° and 1000°C [26, 28].

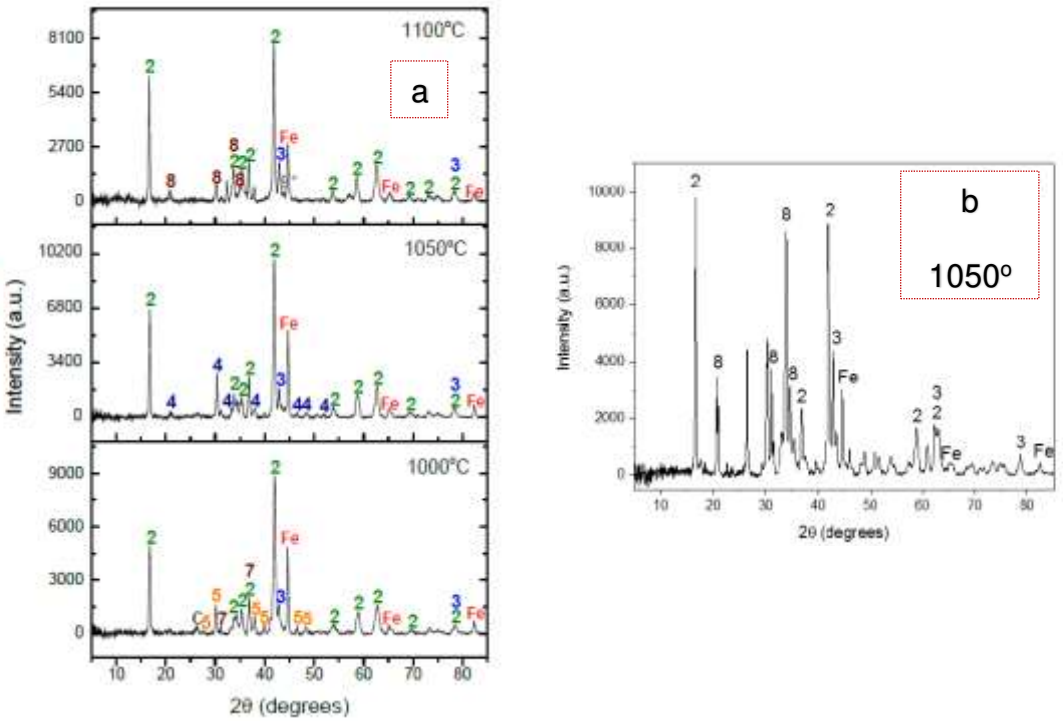

FIGURE 3: A comparison of the X-ray powder diffraction (XRPD) data showing phases formed before and after the reduction reaction of chromite ores (S African, Brazilian). The mixture composition was (chromite:Na_2CO_3:charcoal weight ratio=1:1:0.2). Time (t) 2.5 hours. Reduction atmosphere maintained by flowing argon gas 0.5L min^{-1}. [a] XRPD of S African chromite ore after reduction at temperatures 1000°C, 1050°C and 1100°C. Phases identified are [1-$(Fe_{0.5}Mg_{0.5})(Cr_{0.73}Al_{0.27})_2O_4$, 2-$NaCrO_2$, 3-MgO, 4-$NaAlO_2$, 5-$Na_2CO_3$, 6-$Na_{0.87}Mg_{0.4}Al_{0.07}Si_{0.53}O_2$, 7-$(Fe,Mg)_2SiO_4$, 8-$Na_{1.8}Mg_{0.9}Si_{1.1}O_4$, 9*-$FeC_{0.045}$, Fe-metallic iron, C-carbon]. [b] XRPD of a Brazilian chromite ore after reduction at 1050°C for 2.5 hours (chromite:Na_2CO_3:C = 1:1:0.2). [2=$NaCrO_2$, 3=MgO, 8=$Na_2Mg(SiO_4)$, and Fe]. The peaks not labelled in XRPD of this ore after reduction is for complex and multicomponent (Al, NA, Mg, Ca) silicates which are present in the scanning electron microscopic analysis and maybe partly amorphous. For unreacted S African, and Indonesian ores, the XRPD data are presented in Figures S2 and 3a-3b.

3.4) SEM Image and EDX Analyses of Reduced Chromite Ores: The microstructures of reduced products in the formed in 2g pellets were analysed using SEM and EDX techniques, and the results are compared in **Figures 5a-5d**. These microstructural features are quite distinct from that reported for the oxidative process elsewhere [12].

The EDX maps of elements in **Figures 5a and 5b** help in explaining the chemical dissemination of elements in phases present after reduction. For example, the distribution of Cr^{3+}-ions can be distinguished between the phase microstructures of $NaCrO_2$ (Cr^{3+}-state) and Fe-Cr (Cr^0-state) alloy in **Figures 5a and 5b**. Identification of the morphological difference between metallic and inorganic phases is important for subsequent magnetic phase separation [13].

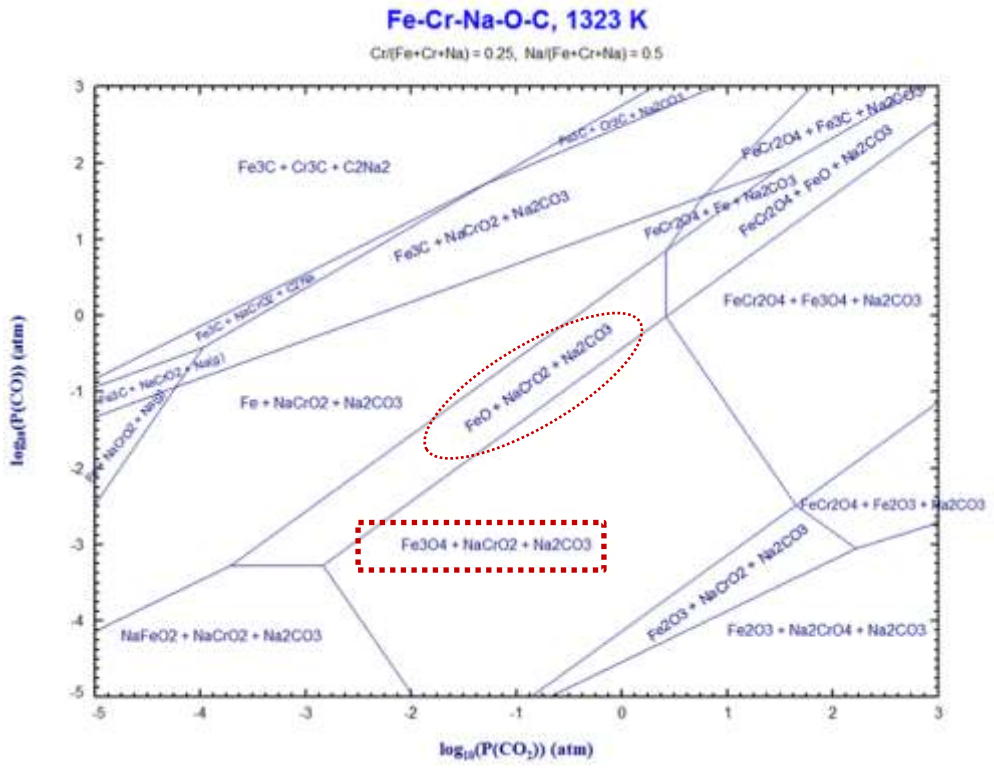

Figure 4: Computed multicomponent phase equilibrium assemblages using the Fact Sage program [23] at 1323K (1050°C) for the Fe-Cr-Na-C-O. Accompanying predominance area diagrams for the Mg-Cr-Na-C-O and Fe-Al-Na-C-O systems are presented in the Supplementary Information.

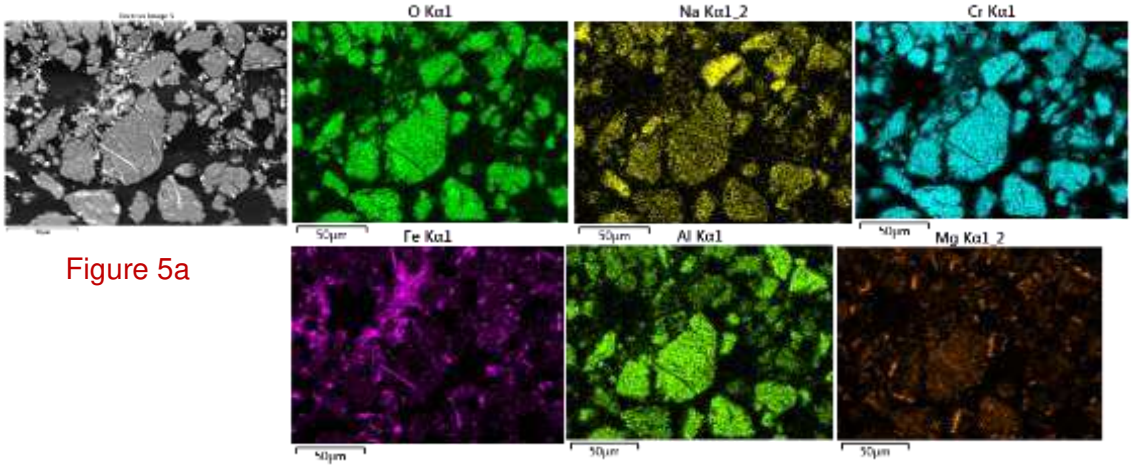

Figure 5a

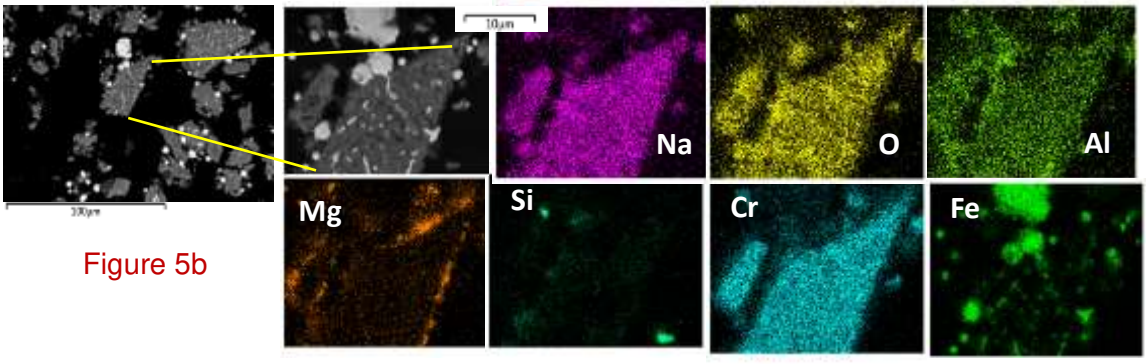

Figure 5b

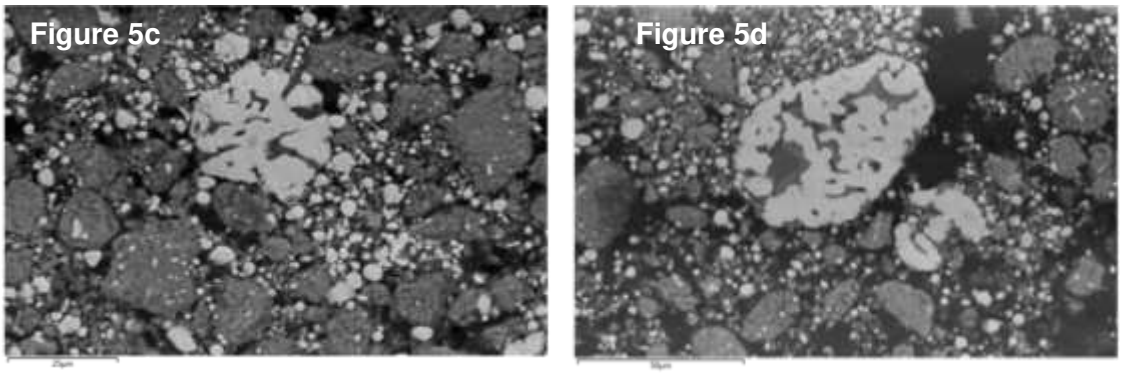

Figure 5: The backscattered electron images of reduced chromite ore particles with energy dispersive X-ray maps of the elemental distributions across the original spinel minerals: a) shows a back-scattered image cross-section with the elemental map of S African chromite spinel reduced at 1323K (1050°C), chromite:Na_2CO_3:C=1:1:0.2. b) shows a back-scattered image cross-section with elemental map of Brazilian chromite reduced at 1323K (1050°C), chromite:Na_2CO_3:C=1:1:0.2. c) 1100°C for 1.5 hours and d) 1200°C for 1 hour are for (S A Chromite).

The large size and irregular morphology of alloy particulates, which are evident in **Figures 5a, 5c and 5d**, enhances the efficiency of magnetic separation of magnetic phase from the reduced S African chromite. The needle-like morphology of alloy formed during the reduction reaction compares well with the microstructure of the decomposed iron oxide formed in the matrix of quaternary spinel present in S African chromite [27] [29]. By contrast, the microstructure of alloy phase is quite finely distributed in the reduced ore matrix. Also, the microstructure shows that the volume fraction of alloy phase in the reduced Brazilian chromite in **Figure 5b** is quite distinct from the structure of the alloy phase in **Figures 5a**. The apparent difference in the fraction of alloy phase formed in each ore is attributed to the concentration of iron and chromium oxides and silica, discussed above in **Table 3**. During reduction reaction, the complex silicates present in chromite combine with alkali above 1000°C and form a low-melting viscous liquid [28] which reduces the diffusive transport of Fe^{2+}/Fe^{3+} ions and oxygen. The slow diffusive transport results into lesser fractions of reduced alloy, which is consistent with a similar observation in iron-making reactions [5,8,30].

When the temperature is increased above 1050°C, the alloy particulates coarsen to larger size, as shown in **Figures 5c** and **5d**. The coarsening of alloy particulates in these two figures occur due to the increased diffusive transport in the silicate liquid at 1100°C and 1200°C, respectively. In this investigation we were unable to characterise the magnetic separation efficiency of the ores accurately because the mass required for analysis was in kilo gram scale. However, from the comparative studies of two ores at 1050°C, it was evident that the alloy phase was much easier to separate from the reduced S African chromite than from the Brazilian chromite.

3.5) Post-reduction ore processing and separation of metallic values

For the post-reduction physical separation of inorganic and metallic phases, $NaCrO_2$ and $NaAlO_2$, and Fe-Cr alloy, respectively, the following steps were adopted: **i**) *wet magnetic*

457 *separation and characterization of magnetic fractions*; **ii**) *aqueous and acid leaching of*
458 *non-magnetic fraction for $NaAlO_2$ and $NaCrO_2$, respectively for reclamation of Al_2O_3 and*
459 *Cr_2O_3, respectively*; and **iii**) *recovery of alkali from sodium aluminate solution by sparging*
460 *with CO_2 gas, produced from the combustion of CO off-gas for energy generation.*

461 3.5.1) Magnetic separation

462 From the analysis of XRPD data, it is evident that besides $NaCrO_2$, the Fe-Cr alloy is
463 another dominant phase in the reduced material, which was separated from the non-
464 magnetic oxide fractions using a wet magnetic separator. Hot water at 50°C was used
465 during the magnetic separation for maximizing the separation of water-soluble $NaAlO_2$,
466 Na_2SiO_3 and unreacted alkali. We observed that the coarse alloy particulates in S African
467 and Indonesian chromites separated much better from the non-magnetic fraction than
468 that observed in the Brazilian ores, in which the alloy particulates were finely distributed.
469 For coarse alloy particles, the separation efficiency was estimated to be ~90% compared
470 with 60% for the fine particle of alloy in the reduced Brazilian chromite.

471 The fraction of water-insoluble non-magnetic oxide was then separated from the alkaline
472 solution by filtering and washing with hot water at 50°C. The alkaline solution containing
473 $NaAlO_2$ and Na_2SiO_3 was processed for selective reclamation of $Al(OH)_3$, silicates and
474 Na_2CO_3.

475 3.5.2) Leaching of non-magnetic fraction in aqueous and acid media

476 The alkaline constituents (Na_2CO_3, $NaAlO_2$ and Na_2SiO_3) of reduced chromite after wet-
477 magnetic separation remain soluble in hot water in the high pH~10 leachate. The excess
478 alkali and water-soluble complexes were separated from the insoluble $NaCrO_2$ by
479 filtering the leachate after magnetic separation. For reducing the process waste and
480 energy cost, the recycling of alkali and reclamation of $Al(OH)_3$ as coproducts is essential.
481 Since the S African chromite ore contains more than 14 weight per cent of alumina for
482 every tonne of ore processed, it is estimated that a maximum of 140kg of alumina may
483 be produced by utilizing ~60.4kg of CO_2 produced from the burnt CO gas. Based on the
484 mass of recoverable alumina, the corresponding mass of CO_2 likely to be sequestrated
485 via the production alumina is less than 8%. The remaining CO_2 from off-gas combustion
486 might be used for recovering remaining alkali, $FeCO_3$, Cr_2O_3 from the leachate, which
487 we aim to quantify in future studies.

488 The (E_H-pH) diagrams for alumina and silica precipitation are shown in SI Figures S6a-
489 S6c [29,31]. Since, most of the iron was removed as alloy, the equilibrium phase analysis
490 was carried out by computing the E_H-pH diagrams for controlling the precipitation
491 reaction. Silica can contaminate Cr_2O_3 and $Al(OH)_3$, if not controlled during selective
492 precipitation in controlled pH media. The condition for pH-control for $Al(OH)_3$ separation
493 is explained in Figures S6a, S6b and S6c [32,33] for the Bayer process. The $Al(OH)_3$
494 was precipitated and separated by sparging CO_2 the $NaAlO_2$-rich solution in the pH range
495 of 6 and 7. The $Al(OH)_3$ precipitated as explained in reaction 10, and the Na_2CO_3 was
496 recovered by drying the solution.

$2NaAlO_2+3H_2O+CO_2(g) = Na_2CO_3+2Al(OH)_3$ (10).

The purity of alumina recovered after a single-step leaching was analysed (in wt%) by XRF. It was found to contain ~81.0% Al_2O_3, ~8.0% SiO_2, 4.5% Na_2O, 3.5% CaO, ~2.0% MgO, 0.6%Cr_2O_3, 0.4%Fe_2O_3. Further purification for alumina may be required, depending on the application.

The Pourbaix (E_H-pH) diagram in **Figure 6** for the Na-Cr-Si-H_2O system explains the phase equilibrium condition for the leaching of $NaCrO_2$ to a compound form of Cr_2O_3. The enriched $NaCrO_2$, recovered after magnetic separation, is insoluble in water, which was washed and dried for phase and composition analysis using the XRPD and XRF technique, respectively. After washing and drying, the $NaCrO_2$ was leached with 0.05 to 0.5M H_2SO_4 in a stirred glass vessel at 50°C for 1.5 hours, after which a deep-green Cr_2O_3 precipitate formed which was washed with hot water at 50°C and dried for chemical and phase analyses. The results are summarised in **Figure 7a** for single-step acid-leaching. It is evident that the recovery of Cr_2O_3 increases from ~75% to ~81% purity for the 0.05M and 0.5M acid concentrations, respectively. After separating Cr_2O_3, the alkali was recovered as Na_2CO_3 from the remaining dilute H_2SO_4 leachate by neutralizing with ammonium carbonate. However, the Na_2SO_4 formed may be used as a coproduct. Alternatively, the alkali may be recovered during Cr_2O_3 precipitation by using the lactic or citric acid.

The residual concentrations of impurity oxides present in the precipitated Cr_2O_3 are shown in Table 4. The XRPD analysis in **Figure 7b** shows the presence of unidentified amorphous phase observed at around $2\theta = 20^o$.

Table 4: Chemical composition of non-magnetic fraction, residue and solution after water leaching analysed by XRF.

wt.%	Cr_2O_3	Fe_2O_3	MgO	Al_2O_3	Na_2O	SiO_2	CaO
Non-mag fraction	50.1	5.16	13.3	7.01	7.42	4.34	0.29
Water-leached precipitate	55.3	5.3	13.2	6.04	1.83	3.64	0.17
Solution after water leaching (dried)	1.6	2.52	0.982	0.981	70.7	4.76	1.48

3.5.3) Utilization of CO_2 process in situ

The reduction of chromite with alkali also offers the opportunity for utilizing CO and CO_2 off-gases (see reactions in Table 2 and 10). The CO gas can be combusted for energy generation. In **Table 5** below, the estimated amount of CO generated from the reduction reactions are reported with the potential combustion enthalpy (MJ). By considering the reactions in Table 5, the mass of CO gas can be estimated for generating energy via complete combustion into CO_2: $CO(g)+0.5O_2(g)=CO_2(g)$. The total energy released from

complete combustion is 10 MJ/kg or 5.2 GJ/tonne of energy, for meeting the overall energy requirement of the process.

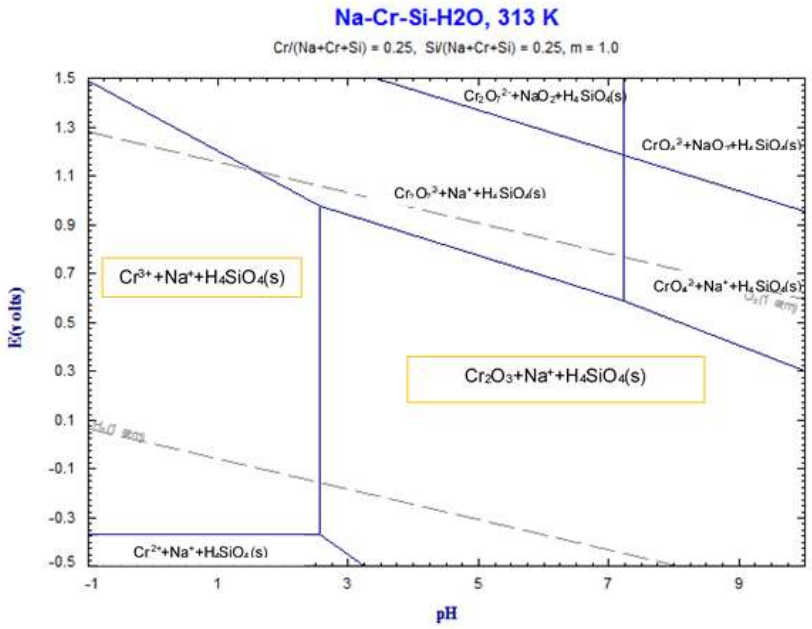

Figure 6: The computed EH-pH diagram for the Na-Cr-Si-H_2O multicomponent system, relevant for chemical separation and purification of Cr_2O_3 and $Al(OH)_3$ from silicate complexes, present in water. See also supplementary information Figures S5a-S5b for alumina and silica precipitation from aqueous media [32,33].

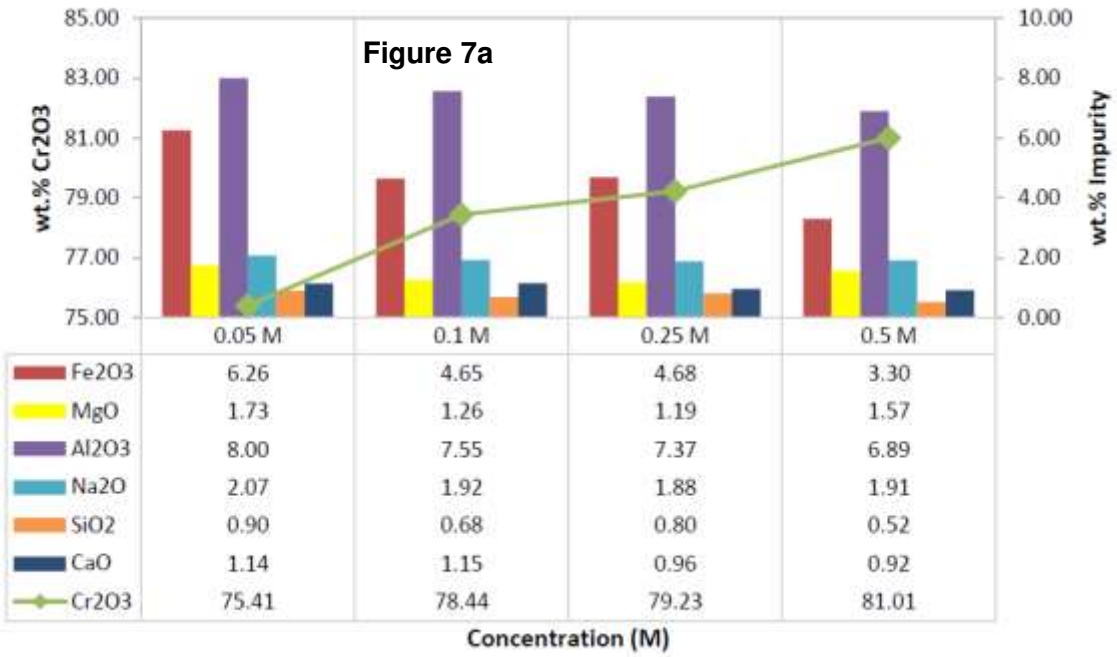

	0.05 M	0.1 M	0.25 M	0.5 M
Fe2O3	6.26	4.65	4.68	3.30
MgO	1.73	1.26	1.19	1.57
Al2O3	8.00	7.55	7.37	6.89
Na2O	2.07	1.92	1.88	1.91
SiO2	0.90	0.68	0.80	0.52
CaO	1.14	1.15	0.96	0.92
Cr2O3	75.41	78.44	79.23	81.01

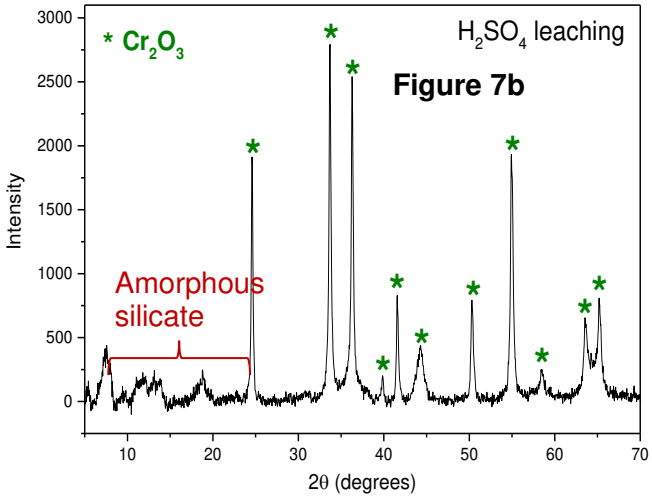

Figure 7: a) Effect of increasing the molar concentrations (0.05 to 0.5M) of sulphuric acid on the purity of Cr_2O_3 leached. b) The Cr_2O_3 powder was analysed by XRF and XRPD, showing Cr_2O_3 phase with unidentified broad peaks below $2\theta=20^o$.

Table 5: Chemical reactions for estimating maximum energy available for **5 tonnes** of S African chromite used in the process. No energy loss is assumed in the process.

Reactions	Oxide, kg	Carbon, kg	CO, kg	Enthalpy, MJ
$Na_2CO_3+Cr_2O_3+C= 2NaCrO_2+2CO$ (g)	2230	176.1	821.6	8216
$Al_2O_3+Na_2CO_3+C=2NaAlO_2+2CO$ (g)	721.5	84.9	396.1	3961
$Na_2CO_3+SiO_2+C= Na_2SiO_3+2CO$ (g)	190	38.0	177.3	1773
$Fe_2O_3+3C=2Fe+3CO$ (g)	1230	260.5	1215.5	12155
Total	4391.5	559.5	2610.5	26105

3.6) Determination of Cr^{6+} ions in leachate solution streams

After wet-magnetic separation and H_2SO_4 leaching of $NaCrO_2$, respectively, the two types of leachates with alkaline pH>8 and acidic pH<4 are produced. These two leachates were analysed for quantifying the presence of residual Cr^{3+} and Cr^{6}+-ions. The acid and alkaline leachates were analysed using the UV-visible absorption spectrophotometry in the 200-700 nm range. In this range, both the Cr^{3+} and Cr^{6+}-ions have strong absorption bands, which can be used for calibrating the concentrations (ppm) using the Lambert-Beers law. The analysis for the presence of the Cr^{3+} and Cr^{6+}-ions in two leachates was carried out after exposing them in open air between two weeks and 6-month period. In **Figures 8a and 8b**, the shape and peak positions of absorbance (A,cm^{-1}) for the Cr^{3+}- and Cr^{6+}-ionic states uniquely characterize the ligand fields in the leachate media which change with pH [32-34]. From Figures S7a and S7b, it is evident that the Cr^{6+}-ions exhibit much larger absorption cross-section in the UV-visible range than that for Cr^{3+}-ions. The strong absorption in Cr^{6+} ions limited the range for concentration calibration up to 20ppm, due to the limitation of the detector sensitivity in the 250-450 nm range.

In **Figures 8c and 8d**, the analysed peaks are compared with the absorbance peaks in **Figures 8a and 8b**, for the alkaline media. From the comparison of apparent absorbance, there appears to be little evidence for the presence of Cr^{6+}- and Cr^{3+} ions in alkaline media. However, in the analysed acid media, the strength of Cr^{6+}-ion absorption peaks at 301 nm were analysed after 2-weeks and 6-months and are shown in **Figure 8c**. These peaks have red-shifted with respect to the 275 nm peak for Cr^{6+}-ions in **Figure 8b**. For the presence of residual Cr^{3+} ion, we characterized the absorption peaks for Cr^{3+}-ion near ~575 nm in **Figure 8d**. The absorbance values were found to be 0.0079 cm^{-1} and 0.0336 cm^{-1} for the two partially oxidized acid leachates. From the calibration equation: $A(cm^{-1}) = 2.602 \cdot 10^{-4} C - 0.0023$, it was concluded that the residual concentrations (C, ppm) of Cr^{3+}-ions in acid solutions after 6 months and two weeks are ~39 ppm and ~138 ppm, respectively.

In Table 6 below, the total concentrations of Cr-ions in each leachate medium was also analysed using the AA spectroscopy. From the calibration curves in Figures S7a and S7b and data in **Figures 8c-8d**, the residual concentrations of Cr^{6+}-ions in acid media after 2 weeks and 6 months were estimated to be 2 ppm and 101 ppm, respectively using the overall Cr-ion mass balance.

Table 6: Analysed composition of the alkaline solutions and acid leachate in ppm using Atomic Absorption Spectroscopic technique

Concentration (ppm)	Cr	Fe	Mg	Al	Na	Si	Ca
Combined alkaline solution	238.1	457.9	16.1	2253.8	20395.3	128.2	28.5
Acid leachate	140.3	358.6	1062.3	223.4	81.3	219.8	2.1

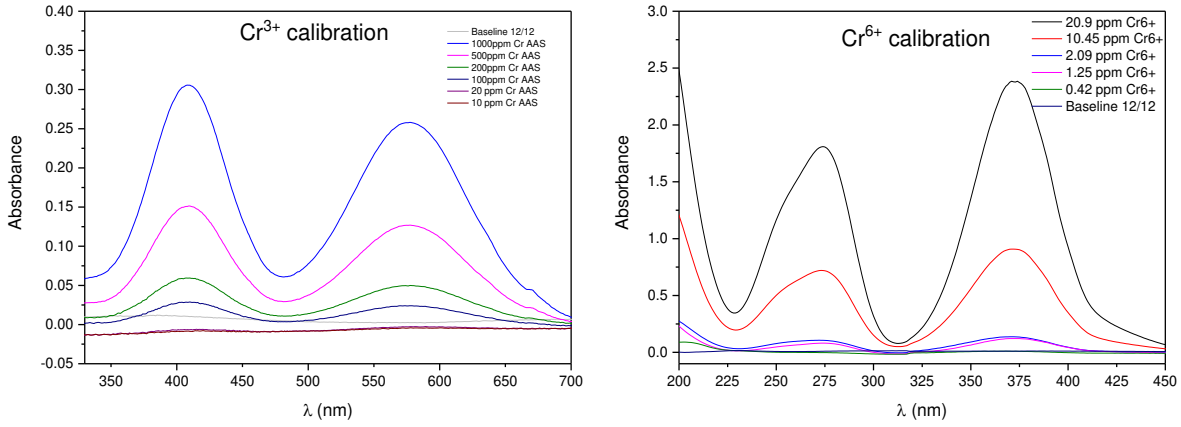

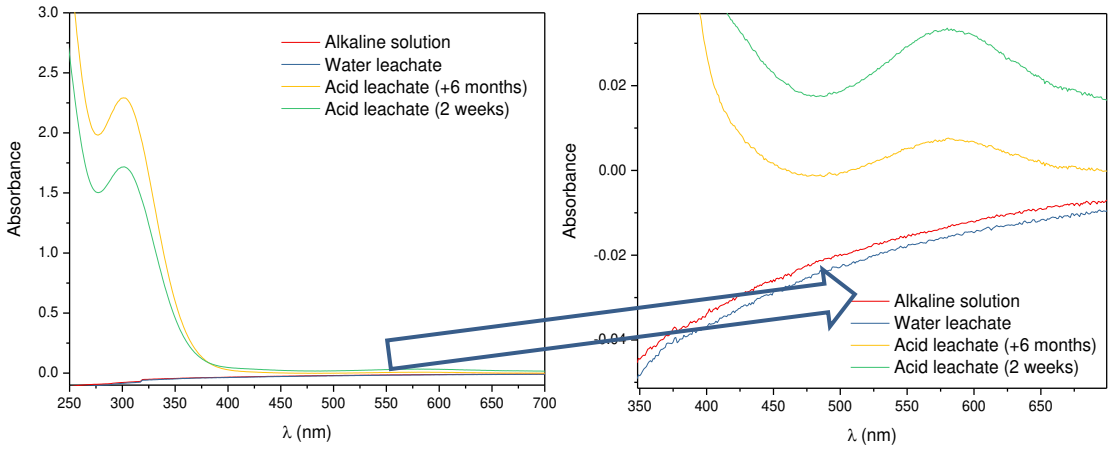

Figure 8: Absorbance (cm^{-1}) versus λ (nm) curves for **a)** Cr^{3+} (concentrations of 1000 ppm, 500 ppm, 200 ppm, 100 ppm, 20 ppm and 10 ppm) and **b)** Cr^{6+} (concentrations of 20.9 ppm, 10.45 ppm, 2.09 ppm, 1.25 ppm and 0.42 ppm) in aqueous media. **(c)** Absorbance versus wavelength UV-vis curves of the alkaline solution from magnetic separation, water leachate and acid leachate analysed in the range of 250-700 nm and, (**d**) Zoomed in area of graph (c). The calibration curves are presented in Figures S7a and S7b.

3.7) A comparative summary of reducibility of chromite ores

As specified in Table 3 we analysed three different types of chromite ores for determining the extraction efficiency of chromium values and coproducts. For the stoichiometric ratio S African chromite:Na_2CO_3:C=1:1:0.2, the investigations on the fractional conversion (%X) in **Figures 2a and 2b**, magnetic separation, and single-step acid leaching with 0.5M H_2SO_4 studies show that the highest yield was for 81% pure Cr_2O_3 and 81% pure Al_2O_3. The purities of Cr_2O_3, Al_2O_3 and Fe-Cr alloy decreased to less than 70% for the Brazilian chromite. The apparent difference is attributed to the presence of high concentrations of silicates which combine with alkali by forming viscous silicate liquid which impedes the overall chemical reaction at elevated temperature. Controlling the kinetics of completion of high-temperature reduction reaction is a critical step in the overall reclamation of metallic values via subsequent magnetic separation and aqueous and acid leaching. The salient differences in the microstructures in **Figures 5a and 5b** explain the mineralogical limitations of the Brazilian chromite for the extraction of chromium chemicals and alloy.

The mineralogical analysis in Table 3 and XRPD also confirm that both the Brazilian and Indonesian chromite ores also have high concentrations of alumina. However, the quantity of extracted alumina from $NaAlO_2$ in Brazilian and Indonesian ores is dependent on the stoichiometric ratio of chromite: Na_2CO_3. By increasing the alkali content in the mixture, the complex aluminium-silicates minerals breakdown at elevated temperature (>1000ºC) and form $NaAlO_2$, which is well understood and reported [11]. For increasing the fractions of chromium chemicals extracted in Brazilian ores, higher than 1:1 ratio of alkali to chromite may be used.

Although in this investigation, we demonstrate the feasibility for the extraction of Fe-Cr alloy, Cr_2O_3 and alumina, future research may be able to focus on process parameter (time, temperature, magnetic separation efficiency) for each ore type, for controlling alloy composition, purities of Cr_2O_3 and alumina, and the residual silicates needed as a feedstock in refractories and cement industries.

3.8 Comparison with oxidative roasting of chromite

The results of alkali-based reduction roasting of chromite ores with carbon differ significantly with the oxidative alkali roasting [10]. The reductive process does not produce COPR, instead it yields valuable co-products, namely Al_2O_3, Fe-Cr alloy and Na_2CO_3. No Cr^{6+}-waste forms as long as the acid leachate after Cr_2O_3 recovery is reused in a closed loop in the process by treating with metallic iron filings [11, 12, 17].

3.9 Energy resources and potential favourable environment impact

The combustion of CO gas from the reactions shown in Table 5 can potentially provide 5.2 GJ/t of energy for the chromite reduction process. The concept of energy generation, CO_2 sequestration by regenerating Na_2CO_3, and Cr^{6+}-free chemical process is far more beneficial for environment and animal beings than the oxidative route to chromate chemicals.

4). Conclusions

a) The alkali reduction of three different types of chromite ores (S African, Brazilian, Indonesian) were investigated for the extraction of Fe-Cr alloy and $NaCrO_2$, as chromium values. The reduction reactions of oxides with carbon, discussed in Table 2, keeps the valence state of chromium in Cr^{3+} and Cr^0 states.

b) The rates of reduction reaction for S African and Brazilian chromite ores with sodium carbonate and carbon, mixed in the stoichiometric ratio of (ore:Na_2CO_3:C=1:1:0.2) were investigated in the 800^{o}C to 1050^{o}C range. The effect of reduction time and temperature on the yield of chromium values were analysed, as compared in **Figures 2a and 2b**. The maximum extent of the overall chemical reaction (%X) at 1050^{o}C was ~70% and 95% for the Brazilian and S African chromites, respectively.

c) The control of reduction time and temperature determines the morphological growth of Fe-Cr alloy particulates. The SEM analysis in Figures 5a, 5c, and 5d show that the average size of alloy particulates increases with temperature during the reduction of S African ore. It was found that the coarsened alloy particulates separate much better than finer particulates. From magnetic separation, the efficiency of separation for coarse and fine alloy particles were estimated to be ~90% and less than 60%, respectively.

d) The wet magnetic separation and water washing increases the concentration of water-soluble products, by leaving behind the insoluble $NaCrO_2$ for further purification via acid

leaching. More than 81% pure $Al(OH)_3$ was precipitated by CO_2 bubbling in the pH range of 6-7, which is necessary for minimizing the co-precipitation of silica. The extraction of $Al(OH)_3$ reduces the amount of waste generated and also helps in recycling CO_2 and regenerating Na_2CO_3 for the process.

e) The extracted $NaCrO_2$ after magnetic separation was leached with the dilute sulphuric acid. The molar strength of acid medium used for the leaching of $NaCrO_2$ at 50^oC was varied between 0.05M and 0.5M. The purity of Cr_2O_3 extracted was dependent on acid strength and varied between 75wt% and 81wt%, as shown in **Figure 7a**.

e) The residual concentration of Cr^{6+}-ions in the spent leachate after Cr_2O_3 recovery was analysed after 2 weeks and 6 months of exposure in air. The concentrations of Cr^{6+}-ions increased from 2 ppm in 2 weeks to 138 ppm in six months. Based on analysis for Cr^{6+} ion in spent leachate, it is recommended that the process liquid is recycled in a close loop for saving water.

f) The reduction reaction with carbon is the main source of CO gas, which is on combustion yields 5.2 GJ of energy for each tonne of ore reduced.

Contributions from each author

See Credit author statement

Acknowledgement

The authors acknowledge financial support from the Leeds Doctoral Training Scholarship, NERC SoS-RARE (NE/M01147X/1) and Catalyst Grants (NE/L002280/1), Marie-Curie IIF E^4-Crit-Mat projects.

References

1. Stringer, J., B.A. Wilcox, and R.I. Jaffee, *The high-temperature oxidation of nickel-20 wt. % chromium alloys containing dispersed oxide phases.* Oxidation of Metals, 1972. **5**(1): p. 11-47.
2. Vardar, E., R.H. Eric, and F.K. Letowski, *Acid leaching of chromite.* Minerals Engineering, 1994. **7**(5): p. 605-617.
3. SC, T. and L. F. *Chromite Ore for the Production of Chromium Chemicals* in *Proceedings of Australian Institute of Mining & Metallurgy,* 1984.
4. Wang, S., et al., *Dehydrogenation of ethane with carbon dioxide over supported chromium oxide catalysts.* 2000. **196**(1): p. 1-8.
5. Tathavadkar V D, A. Jha and M. P. Antony, *The effect of salt-phase composition on the rate of soda-ash roasting of chromite ores*, Metallurgical and Materials Transactions B 2003, **34**, pp.555–563. https://doi.org/10.1007/s11663-003-0024-y
6. Gu, F. and B. Wills, *Chromite-mineralogy and processing.* J Minerals Engineering, 1988. **1**(3): p. 235-240.
7. Jha, A., *The alkali roasting of complex oxide minerals for high purity chemicals-beyond the Le Chatelier era into the 21st century.* J Metals, 2011. **63**(1): p. 39-42.
8. Ji F-Z., S Du and S. Seetharaman, *Experimental Studies of the Viscosities in the CaO-Fe_nO-SiO_2 Slags,* 1997. Metallurgical & Materials Transaction B, 28B, pp. 827-834. https://doi.org/10.1007/s11663-997-0010-x
9. Kowalski, Z. and M. Gollinger-Tarajko, *Environmental evaluation of different variants of the chromium compound production model using chromic waste.* Waste Management, 2003. **23**(8): p. 771-783.
10. Tathavadkar, V.D., M.P. Antony, and A. Jha, *The soda-ash roasting of chromite minerals: Kinetics considerations.* Metallurgical and Materials Transactions B-Process Metallurgy and Materials Processing Science, 2001. **32**(4): pp. 593-602. https://doi.org/10.1007/s11663-001-0115-6
11. Moon, D.H., et al., *Long-term treatment issues with chromite ore processing residue (COPR): Cr6+ reduction and heave.* Journal of Hazardous Materials, 2007. **143**(3): p. 629-635.
12. Antony, M.P., et al., *The soda-ash roasting of chromite ore processing residue for the reclamation of chromium.* Metallurgical and Materials Transactions B-Process Metallurgy and Materials Processing Science, 2001. **32**(6): p. 987-995. https://doi.org/10.1007/s11663-001-0087-6
13. Sun, Z., et al., *A new method of potassium chromate production from chromite and KOH-KNO3-H2O binary molten salt system.* AIChE Journal, 2009. **55**(10): p. 2646-2656.
14. Sun, Z., et al., *Oxidation decomposition of chromite ore in molten potassium hydroxide.* International Journal of Mineral Processing, 2007. **83**(1-2): p. 60-67.
15. 2017, U.S.E.P.A., *Chromium in Drinking Water.* 2017.
16. (Geneva), W.H.O., *Guidelines for drinking-water quality*. 2004, WHO: Geneva. p. 13.

17. Nickens, K.P., S.R. Patierno, and S. Ceryak, *Chromium genotoxicity: A double-edged sword.* Chemico-Biological Interactions, 2010. **188**(2): p. 276-288.

18. Chase, M.W., *NIST-JANAF Thermochemical Tables 2 Volume-Set (Journal of Physical and Chemical Reference Data Monographs)*. NIST-JANAF Thermochemical Tables, 4th Edition ed. NIST-JANAF Thermochemical data. 1998: American Institute of Physics.

19. Kubaschewski, O. and C.B. Alcock, *Metallurgical thermochemistry*. 5th (Revised & Enlarged) ed. International Series on Materials Science and Technology, ed. G.V. Raynor. Vol. 24. 1979, Oxford: Pergammon International Library.

20. Turkdogan, E.T., *Physical Chemistry of High Temperature Technology*. 1980, New York: Academic Press 447.

21. Bale, C., A. Pelton, and W. Thompson, *FACT Sage*. 1976-2013, Thermfact/CRCT and GTT-Technologies.

22. Roine, A., *Chemistry for Windows: Chemical Reaction and Equilibrium Software with Extensive Thermodynamical Database*, H.S.C, Editor. 2002: Outokumpu Research Oy, Finland.

23. Escudero-Castejon, L., et al., *Formation of Chromium-Containing Molten Salt Phase during Roasting of Chromite Ore with Sodium and Potassium Hydroxides.* Journal for Manufacturing Science and Production, 2016. **16**(4): p. 11.

24. Parirenyatwa, S., et al., *Comparative study of alkali roasting and leaching of chromite ores and titaniferous minerals.* Hydrometallurgy, 2016. **165**: p. 213-226.

25. Chrysochoou, M. and D. Dermatas, *Application of the Rietveld method to assess chromium(VI) speciation in chromite ore processing residue.* Journal of Hazardous Materials, 2007. **141**(2): p. 370-377.

26. Narkiewicz, U., et al., *Nucleation of the Fe_3C in the reaction of methane with nanocrystalline iron.* Journal of Materials Research, 2005. **20**(2): p. 386-393.

27. Navrotsky, A., *Physics and Chemistry of Earth Materials. Cambridge Topics in Mineral Physics and Chemistry* 2009/05/01 ed. Geological Magazine, ed. A. Pring. Vol. 6. 1996: Cambridge University Press. 447.

28. Tathavadkar, V.D., M.P. Antony, and A. Jha, *The physical chemistry of thermal decomposition of South African chromite minerals.* Metallurgical and Materials Transactions B-Process Metallurgy and Materials Processing Science, 2005. **36**(1): p. 75-84. https://doi.org/10.1007/s11663-005-0008-1

29. Davoodi, A., et al., *Multianalytical and In Situ Studies of Localized Corrosion of EN AW 3003 Alloy - Influence of Intermetallic Particles.* Journal of The Electrochemical Society 2008. **155**: p. 138-146.

30 Seok Seong-Ho, Jung S-M, Lee Y-S L and Min, D-J, *Viscosity of Highly Basic Slags,* ISIJ International, Vol. 47 (2007), No. 8, pp. 1090–1096. https://doi.org/10.2355/isijinternational.47.1090

31. Nikolaychuk, P.A., *The revised Pourbaix diagram for silicon.* Silicon, 2014. **6**(2): p. 109-116.

774 32. Burns, R.G., *Mineralogical Applications of Crystal Field Theory*. Cambridge
775 Topics in Mineral Physics and Chemistry, ed. A.P.a.R.C. Liebermann. 1970,
776 Cambridge: Cambridge University Press. 241-284.
777 33. Cotton, F.A. and G. Wilkinson, *Advanced Inorganic Chemistry*. 3rd ed. 1962,
778 New York: Interscience Publisher. 831-841.
779 34. Paul, A., *Chemistry of Glasses*. 1st ed. 1982: Chapman & Hall. 148-173.